

# UC Davis

## UC Davis Previously Published Works

### Title

Optimization of the resampling method in the weighted ensemble simulation toolkit with parallelization and analysis (WESTPA)

### Permalink

<https://escholarship.org/uc/item/7rt270s7>

### Journal

The Journal of Chemical Physics, 161(4)

### ISSN

0021-9606

### Authors

Plotnikov, Dennis

Ahn, Surl-Hee

### Publication Date

2024-07-28

### DOI

10.1063/5.0197141

### Copyright Information

This work is made available under the terms of a Creative Commons Attribution License, available at <https://creativecommons.org/licenses/by/4.0/>

Peer reviewed

BRIEF REPORT | JULY 22 2024

## Optimization of the resampling method in the weighted ensemble simulation toolkit with parallelization and analysis (WESTPA) **FREE**

Dennis Plotnikov  ; Surl-Hee Ahn  




*J. Chem. Phys.* 161, 046101 (2024)

<https://doi.org/10.1063/5.0197141>



22 July 2024 18:29:12




**The Journal of Chemical Physics**

**Special Topic:**  
**Dynamic Exciton for Materials, Biology  
and Energy Conversion**

Guest Editors: Hiroshi Imahori, Prashant Kamat, Hironori Kaji, Yasuhiro Kobori, Kiminori Maeda, Michael R. Wasielewski  
JCP Editors: Tianquan (Tim) Lian, Renee Frontiera, Jennifer Ogilvie, Qiang Shi

**Submit Today!**



# Optimization of the resampling method in the weighted ensemble simulation toolkit with parallelization and analysis (WESTPA)

Cite as: J. Chem. Phys. 161, 046101 (2024); doi: 10.1063/5.0197141

Submitted: 11 January 2024 • Accepted: 9 July 2024 •

Published Online: 22 July 2024



View Online



Export Citation



CrossMark

Dennis Plotnikov  and Surl-Hee Ahn<sup>a)</sup> 

## AFFILIATIONS

Department of Chemical Engineering, University of California, Davis, Davis, California 95616, USA

<sup>a)</sup> Author to whom correspondence should be addressed: [sahn@ucdavis.edu](mailto:sahn@ucdavis.edu)

Published under an exclusive license by AIP Publishing. <https://doi.org/10.1063/5.0197141>

Molecular dynamics (MD) simulations are powerful tools for studying the dynamic behavior of molecular systems at the atomic level. MD simulations provide insights into the structural, thermodynamic, and kinetic properties of a wide range of systems such as proteins,<sup>1–3</sup> protein–ligand systems,<sup>4–6</sup> membrane–ligand systems,<sup>7–10</sup> and polymers.<sup>11–14</sup> However, one of the major challenges in MD simulations is the exploration of rare events or long timescale phenomena, which are often computationally intractable and beyond the reach of conventional MD simulations. To address this challenge, “enhanced sampling methods” have been developed by several researchers and are often used to sample thermodynamic and/or kinetic properties efficiently from MD simulations.

Enhanced sampling methods can be broadly categorized into three kinds of methods: (1) those that add a biasing potential or change the temperature of the system to sample thermodynamic properties,<sup>15–19</sup> (2) those that focus on sampling transition paths and rate constants between two states of interest,<sup>20–22</sup> and (3) those that focus on sampling thermodynamic and kinetic properties of the configuration space by dividing up the configuration space into small volume elements (“macrostates” or “bins”) with chosen progress coordinate(s) and calculating transitions between different macrostates or bins.<sup>23,24</sup> Weighted ensemble (WE) is one of the methods in the second and third categories that runs multiple short trajectories with probabilities in parallel and periodically merges or replicates trajectories in each bin.<sup>23,25</sup> The bins are constructed so that they effectively bridge different probability density regions when running the WE simulations. This approach allows for an efficient exploration of the configuration space and directly provides unbiased thermodynamic and kinetic properties since it does not add a statistical bias to the system. WE has been used to study protein–protein interactions,<sup>26</sup> the receptor binding domain

opening mechanism for the SARS-CoV-2 spike protein,<sup>27–29</sup> membrane permeability of drug-like molecules,<sup>30</sup> and other important biophysical phenomena.

In the original Huber and Kim’s WE, trajectories with probabilities or “weights” are periodically merged or replicated or “resampled” in each bin by the following protocol.<sup>23</sup> First, the number of trajectories in each bin is adjusted to end up with approximately the same number of trajectories, which is similar to setting the target number of trajectories per bin ( $n_t$ ) *a priori* as done in current WE approaches. Then, the total probability  $P_i$  for each visited bin  $i$  is computed from summing all the weights of the trajectories in each bin. The “ideal” trajectory weight is  $P_i/n_t$ . Trajectories with a weight greater than  $2P_i/n_t$  are split into  $m$  trajectories with a weight equal to  $1/m$  of the parent trajectory.  $m$  is chosen so that each child trajectory has a weight between  $P_i/n_t$  and  $2P_i/n_t$ . Then, the trajectories are sorted in ascending order of weights. The trajectories with small weights are combined in a statistically correct way, i.e., the weights are added up, and the total weight is given to the trajectory that is chosen proportionally to its original weight. For example, when combining a trajectory with a weight of 0.01 and a trajectory with a weight of 0.02, the first trajectory has a 1/3 chance of being chosen and the second trajectory has a 2/3 chance of being chosen. The trajectories are combined until either (1) the next trajectory has a weight greater than  $P_i/2n_t$  or (2) the combined weight is greater than  $P_i/n_t$ , in which case the combination is terminated. In the first case, the trajectories will be combined with the next trajectory if the combined weight is  $3P_i/2n_t$  or less. In the end, WE generates  $n_t$  trajectories with weights that are roughly the same or close to the ideal weight in each visited bin, and the bin weights are preserved.

By merging trajectories, the computational cost in sampling frequently sampled, low energy regions gets reduced, whereas by

replicating trajectories, the computational power is geared toward sampling rarely sampled, high energy regions. Thus, from the resampling method, WE is able to obtain sampling efficiency without adding any statistical bias. However, even though the weights are roughly the same or close to the ideal weight, the resampling method ends up generating statistical errors by generating trajectories with unequal weights. Hence, we have developed a new software implementation of the equal weight resampler that generates trajectories with equal, ideal weights and makes the variance of the weights zero in each bin, which reduces statistical errors. The equal weight resampler implementation can be used with the weighted ensemble simulation toolkit with parallelization and analysis (WESTPA), a widely used software application for running WE simulations.<sup>31–34</sup> The idea of resampling and generating trajectories with equal weights has been suggested by Darve and Izaguirre (Chap. 7 in Schlick<sup>35</sup>) and Aristoff and Zuckerman<sup>36,37</sup> and has been implemented in the concurrent adaptive sampling (CAS) algorithm, an adaptive, high-dimensional variation of WE.<sup>38,39</sup> Although the equal weight resampler in the CAS algorithm generates trajectories with equal, ideal weights, the variance of weights becomes zero in each bin, and the statistical errors are minimized, the resampler in the CAS algorithm introduces a subtle bias. The resampler in the CAS algorithm selects trajectories to merge or split in order from a list of trajectories sorted in descending order of weights. This leads to selecting trajectories with large weights first and having those trajectories predominantly survive in the resampling process, which leads to a subtle bias toward the trajectories with large weights.

Hence, we present a new software implementation of the equal weight resampler that uses the cumulative distribution function (CDF) to select trajectories with replacement to merge or split in an unbiased, probabilistic way and follows Aristoff and Zuckerman's algorithm,<sup>36,37</sup> which has not been implemented anywhere yet. Specifically, the CDF is created based on the trajectories in each bin by first arranging them in ascending order based on their weights. Then, the trajectories' weights are normalized, and those normalized weights are used to sum the weights cumulatively and create a CDF based on the cumulative weights. Then, a random number is computed between 0 and 1 and is mapped to the generated CDF to select a trajectory with replacement. This process is repeated until we have selected a number of trajectories equal to  $n_t$ . Finally, the selected trajectories are assigned the equal, ideal weight so that all trajectories in the bin have equal, ideal weights. However, note that resampling is skipped for a bin if all trajectories have equal, ideal weights since that indicates that there was no bin-to-bin transition, and thus, resampling becomes redundant and the weights would not be changed for the trajectories. (The CDF based on equal weights would be a straight line with a slope of 1 from 0 to 1, and the selection process would not alter the distribution and yield the same trajectories.) Taken together, we aim to improve the accuracy and reliability of the WE simulation results with our equal weight resampler.

To test and compare our equal weight resampler ("equal weight") with the original Huber and Kim resampler ("standard"), two systems were selected: a one-dimensional sinusoidal system governed by over-damped Langevin dynamics taken from <https://github.com/atbogetti/odld/tree/main> and the molecular association of  $\text{Na}^+$  and  $\text{Cl}^-$  ions in explicit solvent, which was taken from the WESTPA tutorials.<sup>33,34</sup> All systems were run with WESTPA 2.0, and the Amber 20 MD engine was used for

the  $\text{Na}^+/\text{Cl}^-$  system.<sup>33,34,40</sup> The total simulation time for the one-dimensional sinusoidal system was  $1.65 \times 10^6 \delta t$  (fixed time interval of  $\delta t = 5 \times 10^{-5}$ ), and the total simulation time for the  $\text{Na}^+/\text{Cl}^-$  system was  $0.25 \mu\text{s}$ . Ten independent simulations were run for the one-dimensional sinusoidal system, and five independent simulations were run for the  $\text{Na}^+/\text{Cl}^-$  system. The WESTPA analysis tools were used to generate the free energy landscape and probability flux or rate constant graphs. The main criteria for assessing our equal weight resampler performance were the error bars (representing 95% confidence intervals) for the data generated from the simulations and the simulation time to reach convergence for the free energy landscapes and probability fluxes or rate constants.

The one-dimensional sinusoidal system has a potential  $V(x)$  described by the following equation:

$$\frac{V(x)}{k_B T} = -15\pi \cos(x) \ln(e^{0.5x} - 1) + \frac{15}{2} \sin(x) \ln(e^{0.5x} - 1), \quad (1)$$

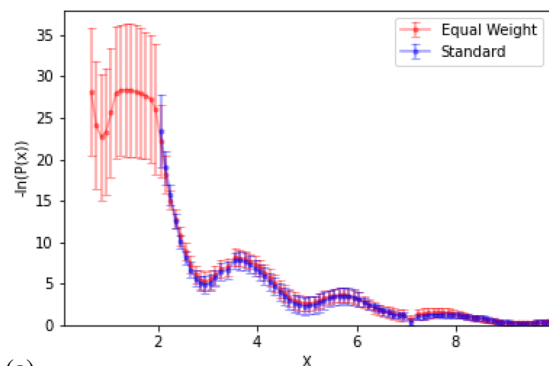
where  $x$  denotes the one-dimensional  $x$ -coordinate,  $k_B$  denotes the Boltzmann constant, and  $T$  denotes the temperature.

The one-dimensional sinusoidal system dynamics are governed by over-damped Langevin dynamics described by the following equation:

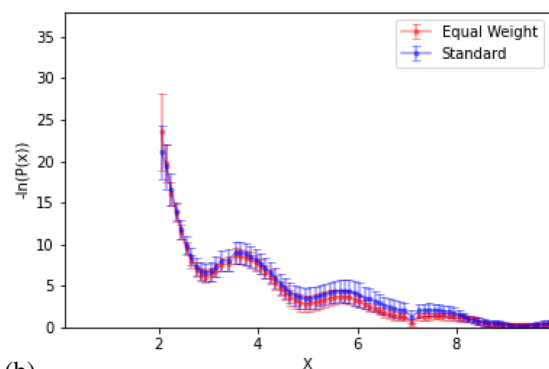
$$x(t + \delta t) = x(t) - \frac{\delta t}{\gamma} \nabla_x V + \delta x^G, \quad (2)$$

where  $\delta t$  denotes the time step,  $\gamma$  denotes the friction coefficient,  $\nabla_x V$  denotes the force calculated from the gradient of the potential  $V(x)$ , and  $\delta x^G$  denotes a Gaussian random displacement with zero mean and  $\frac{2k_B T \delta t}{\gamma}$  variance. Here, we have  $\gamma = 1$  and  $k_B T = 1$  in reduced units and  $\delta t = 5 \times 10^{-5}$ . The progress coordinate was set to be  $x$  for this particular system, and the bins divided  $x$  ranging from 0 to 10 with a spacing of 2, with the minimal adaptive binning (MAB) scheme used to create ten bins between  $x = 2$  and  $x = 6$  so that the probability fluxes between the two metastable states at  $x = 3$  and  $x = 5$  could be calculated efficiently.<sup>41</sup> Although the MAB scheme constructs bins at every iteration adaptively, the change of bins is not a concern since many replicate simulations were run for each system to obtain the free energy landscapes and rate constants and the simulation setup was identical except for the resampler itself. As the MAB scheme focuses on surmounting energy barriers, MAB allows users to obtain free energy landscapes and rate constants more efficiently compared to standard, fixed manual binning schemes.<sup>41</sup> The target number of trajectories per bin  $n_t$  was set to 5, and equilibrium WE simulations were run for this particular system starting from  $x = 9.5$ .

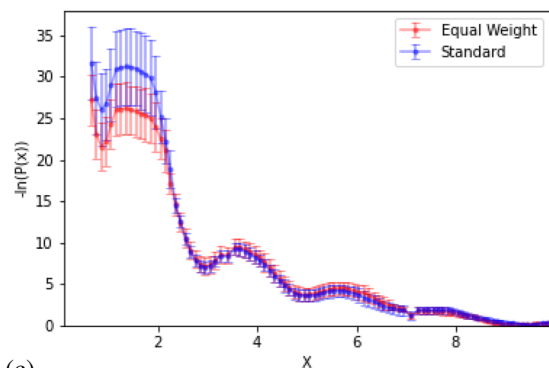
With the one-dimensional sinusoidal system, we also tested the impact of bin count and target number of trajectories per bin  $n_t$ . That is, we increased the number of MAB bins that cover from  $x = 2$  to  $x = 6$  from 10 to 20 for one set of simulations and increased  $n_t$  from 5 to 10 for another set of simulations and tested each impact on both resamplers' sampling of the free energy landscape. Figures 1 and S1 of the [supplementary material](#) show that the equal weight resampler consistently maintains lower or comparable error bars throughout the entire simulation compared to the standard resampler for the free energy landscapes of the one-dimensional sinusoidal system plotted along the progress coordinate  $x$ , which demonstrates the benefit of using the equal weight resampler over the standard



(a)



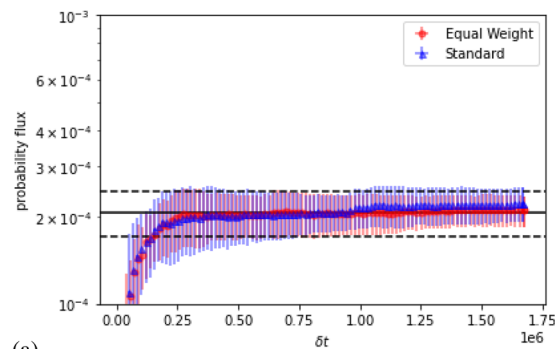
(b)



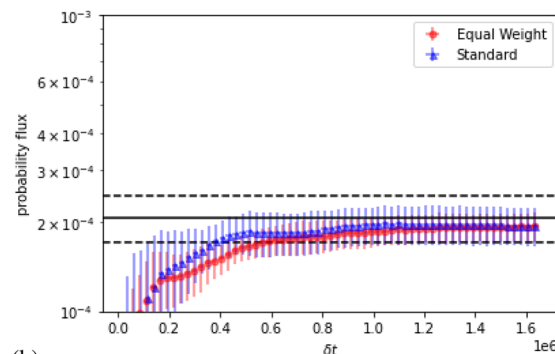
(c)

**FIG. 1.** Free energy landscapes for the one-dimensional sinusoidal system from using the standard resampler (in blue) and the equal weight resampler (in red) at  $25\,000\ \delta t$ . (a) Free energy landscape with 10 MAB bins that cover from  $x = 2$  to  $x = 6$  and the target number of trajectories per bin  $n_t$  set at 5. (b) Free energy landscape with 20 MAB bins that cover from  $x = 2$  to  $x = 6$  and  $n_t$  set at 5. (c) Free energy landscape with 10 MAB bins that cover from  $x = 2$  to  $x = 6$  and  $n_t$  set at 10. The free energy landscapes represent the average free energy landscape, and the error bars represent the 95% confidence intervals calculated from ten independent simulations.

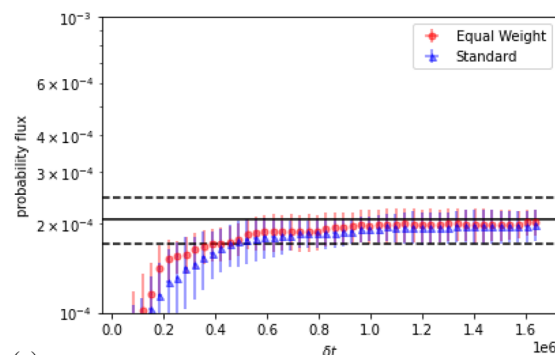
resampler to obtain free energy landscapes with lower simulation errors. In addition, by  $25\,000\ \delta t$ , the equal weight resampler is able to explore the high energy region from  $x = 0$  to  $x = 2$ , whereas the standard resampler is able to sample the same region at later simulation times, as seen in Figs. 1 and S1 of the [supplementary material](#). The accelerated sampling from the equal weight resampler could be



(a)



(b)



(c)

**FIG. 2.** Evolution of the probability flux from  $x = 5$  to  $x = 3$  in the one-dimensional sinusoidal system over  $1.65 \times 10^6\ \delta t$  for both resamplers. (a) Probability flux with 10 MAB bins that cover from  $x = 2$  to  $x = 6$  and the target number of trajectories per bin  $n_t$  set at 5. (b) Probability flux with 20 MAB bins that cover from  $x = 2$  to  $x = 6$  and  $n_t$  set at 5. (c) Probability flux with 10 MAB bins that cover from  $x = 2$  to  $x = 6$  and  $n_t$  set at 10. The markers represent the average probability flux, and the error bars represent the 95% confidence intervals calculated from ten independent simulations. The reference probability flux was  $2.1 \times 10^{-4} \pm 3.74 \times 10^{-5}$ , which was computed based on three independent conventional simulations over  $1.65 \times 10^6\ \delta t$ .

due to having rarer trajectories, once chosen, survive at a higher rate by having equal weights as the rest of the trajectories. In contrast, rarer trajectories would most likely not be chosen from the merging step or not survive at the next iteration by having less than the ideal weight in the standard resampler.

When  $n_t$  was doubled, the equal weight resampler was also able to explore the high energy region from  $x = 0$  to  $x = 2$  more quickly

by  $10\,000 \delta t$  compared to the standard resampler by  $15\,000 \delta t$  (data not shown), so both resamplers show the sampling of the high energy region in Fig. 1. In addition, the equal weight resampler samples the high energy region more accurately at a lower free energy and earlier in the simulation than the standard resampler, which is evident when comparing it with the converged free energy landscape at longer simulation times as seen in Fig. S1 of the supplementary material. However, when the number of bins was doubled, the equal weight resampler was not able to explore the high energy region from  $x = 0$  to  $x = 2$  more quickly than the standard resampler. Both resamplers were able to sample the high energy region eventually by  $35\,000 \delta t$ , but neither resampler was faster at sampling the high energy region than the other (data not shown). The lack of accelerated sampling from the equal weight sampler in this case could be due to the increased number of bins bridging the different probability regions more effectively and lessening the benefits of setting trajectories to have equal weights as a result. At later simulation times, the free energy landscapes from both resamplers became comparable, as seen in Fig. S1 of the supplementary material. Nevertheless, using the equal weight resampler to sample high energy barrier regions more accurately and quickly and obtaining lower simulation errors, especially during early simulation times, will be useful for systems that are computationally expensive to run.

Next, the sampling of the probability fluxes was tested for both resamplers in the original setup and in the two different system

setups (i.e., doubled number of bins and doubled target number of trajectories per bin  $n_t$ ). Figures 2, S2, and S3 of the supplementary material compare the evolution of the probability flux from  $x = 3$  to  $x = 5$ , from  $x = 5$  to  $x = 3$ , and from  $x = 1$  to  $x = 3$ , respectively, in the one-dimensional sinusoidal system over  $1.65 \times 10^6 \delta t$  for both resamplers, in the original setup, and in the two different system setups. The reverse probability flux from  $x = 3$  to  $x = 1$  could not be obtained due to the insurmountable high energy barrier. The state definitions for  $x = 3$ ,  $x = 5$ , and  $x = 1$  are  $2.75 \leq x \leq 3.25$ ,  $4.75 \leq x \leq 5.25$ , and  $0 \leq x \leq 1$ , respectively. Table I shows the final probability fluxes with the relative errors under all different system setups. Both resamplers converge to a stable probability flux value at a similar simulation time, which was determined from visual inspections of the graphs in Figs. 2, S2, and S3 of the supplementary material. Table I shows that the equal weight resampler consistently yields probability fluxes with lower relative errors than the standard resampler for all cases, which demonstrates the benefit of using the equal weight resampler over the standard resampler to obtain probability fluxes with lower simulation errors. The relative errors are slightly lower for the equal weight resampler compared to those for the standard resampler for the  $x = 3$  to  $x = 5$  and the  $x = 5$  to  $x = 3$  transitions since the energy barrier between the two regions is relatively low. For the  $x = 1$  to  $x = 3$  transition, however, the equal weight resampler yields a probability flux with a significantly lower relative error since the associated energy barrier is much higher. When

**TABLE I.** Final probability fluxes for the one-dimensional sinusoidal system under different system setups, which represent the average final probability flux from ten independent simulations. The error bars represent the 95% confidence interval calculated from ten independent simulations.

Transitions	Resampler	Probability flux	Relative error (%)
Original setup			
$x = 5 \rightarrow x = 3$	Standard	$0.000\,22 \pm 3 \times 10^{-5}$	13.6
	Equal weight	$0.000\,21 \pm 2.5 \times 10^{-5}$	12
$x = 3 \rightarrow x = 5$	Standard	$5.4 \times 10^{-5} \pm 7.13 \times 10^{-6}$	13
	Equal weight	$5.22 \times 10^{-5} \pm 3.86 \times 10^{-6}$	7.4
$x = 1 \rightarrow x = 3$	Standard	$7 \times 10^{-8} \pm 7.8 \times 10^{-8}$	111
	Equal weight	$7.9 \times 10^{-8} \pm 4.46 \times 10^{-8}$	56
Doubled number of bins			
$x = 5 \rightarrow x = 3$	Standard	$0.0002 \pm 2.9 \times 10^{-5}$	14.5
	Equal weight	$0.0002 \pm 2.1 \times 10^{-5}$	10.5
$x = 3 \rightarrow x = 5$	Standard	$5.08 \times 10^{-5} \pm 7.7 \times 10^{-6}$	15
	Equal weight	$5.4 \times 10^{-5} \pm 6.5 \times 10^{-6}$	12
$x = 1 \rightarrow x = 3$	Standard	$6.1 \times 10^{-8} \pm 3.2 \times 10^{-8}$	53
	Equal weight	$9 \times 10^{-8} \pm 3.7 \times 10^{-8}$	41
Doubled target number of trajectories per bin			
$x = 5 \rightarrow x = 3$	Standard	$0.0002 \pm 2 \times 10^{-5}$	12
	Equal weight	$0.0002 \pm 2.41 \times 10^{-5}$	10
$x = 3 \rightarrow x = 5$	Standard	$4.9 \times 10^{-5} \pm 9 \times 10^{-6}$	18.4
	Equal weight	$4.5 \times 10^{-5} \pm 6.9 \times 10^{-6}$	15.3
$x = 1 \rightarrow x = 3$	Standard	$5.9 \times 10^{-8} \pm 5.9 \times 10^{-8}$	100
	Equal weight	$7.1 \times 10^{-8} \pm 2.2 \times 10^{-8}$	31

the number of bins was doubled, the relative errors for the equal weight resampler became closer to those for the standard resampler, and the equal weight resampler's performance was worse, except for the  $x = 5$  to  $x = 3$  transition. As previously seen for the sampling of the free energy landscape, the increased number of bins again lessened the benefits of setting trajectories to have equal weights. Meanwhile, when  $n_t$  was doubled, the relative errors for the equal weight resampler became lower than those for the standard resampler, and the equal weight resampler's performance was improved, except for the  $x = 3$  to  $x = 5$  transition. Similar to what was observed for the sampling of the free energy landscape, increasing  $n_t$  proliferated the benefits of using the equal weight resampler by having more trajectories with equal, ideal weights.

The  $\text{Na}^+/\text{Cl}^-$  system was used as the final test system for the equal weight resampler, which consisted of a single  $\text{Na}^+$  cation and a single  $\text{Cl}^-$  anion with Joung and Cheatham parameters<sup>42</sup> and TIP3P water molecules<sup>43</sup> solvating the two ions. The ions were initially separated by 12 Å (unbound state is defined as 10 Å or higher). The progress coordinate was set to be the center of mass distance between the  $\text{Na}^+$  and  $\text{Cl}^-$  ions in Å (denoted as  $x$ ) for this particular system, and 28 MAB bins were used from 2.7 to 20 Å, same as in the MAB

work.<sup>41</sup> The target number of trajectories per bin  $n_t$  was set to 4, and the simulation time for each trajectory was set to 2 ps. Steady-state WE simulations were run for this particular system, where the target state was defined as the bound state (systems with distances lower than 2.7 Å). The rate constants were calculated using the rate event duration (RED) scheme<sup>44</sup> to better estimate the rate constants from pre-steady-state WE simulations, and the unbound state was defined to be systems with distances higher than 15 Å.

As previously done for the one-dimensional sinusoidal system, we first compared the resamplers' performance in sampling the free energy landscape of the  $\text{Na}^+/\text{Cl}^-$  system. Similar to what was observed for the one-dimensional sinusoidal system, Fig. 3 shows that the equal weight resampler consistently maintains lower or comparable error bars throughout the simulation compared to the standard resampler for the free energy landscapes of the  $\text{Na}^+/\text{Cl}^-$  system plotted along the progress coordinate  $x$ . In addition, the equal weight resampler samples the region from 4 to 11 Å more accurately at a higher free energy than the standard resampler at 25 ns, which is evident when comparing it with the converged free energy landscape at longer simulation times as seen in Fig. 3. Note that the free energy landscapes in Fig. 3 are only obtained from

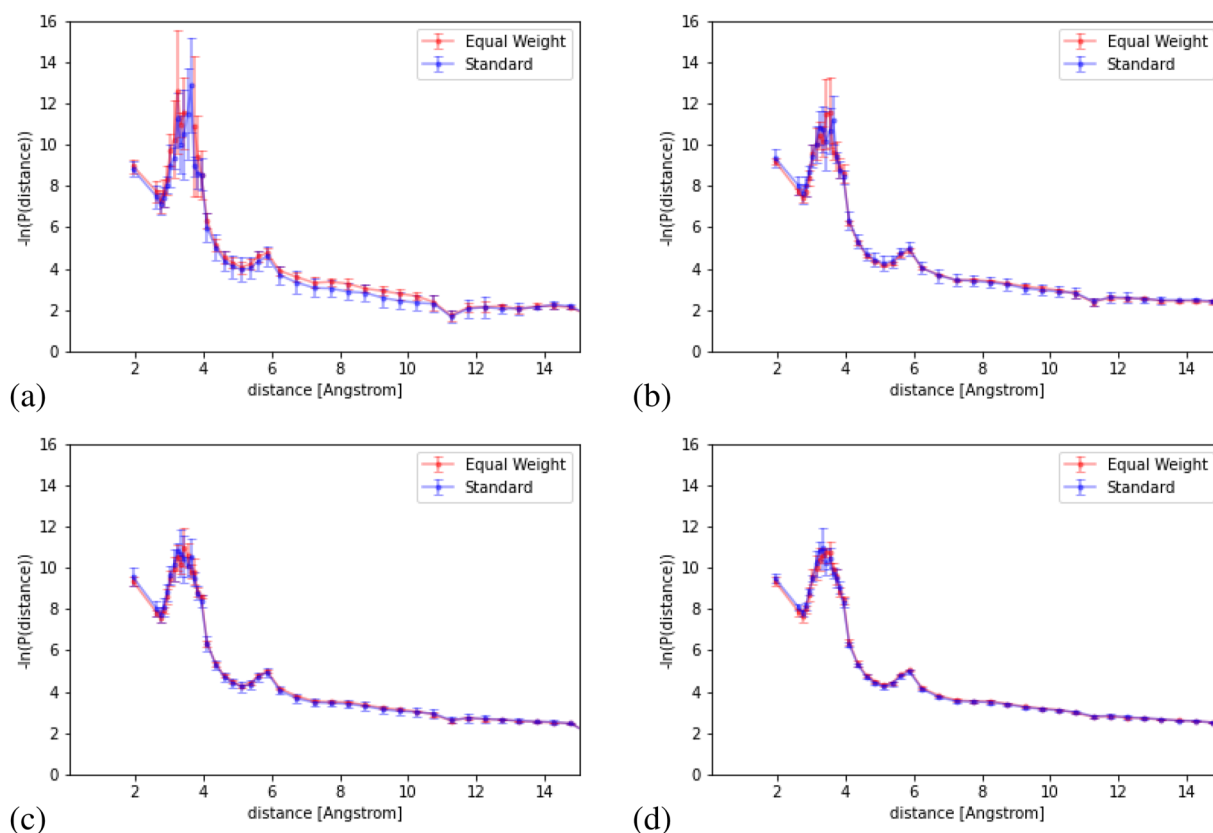


**FIG. 3.** Free energy landscapes for the  $\text{Na}^+/\text{Cl}^-$  system from using the standard resampler (in blue) and the equal weight resampler (in red), where (a), (b), (c), and (d) show the free energy landscapes at 25, 75, 125, and 250 ns, respectively. The free energy landscape represents the average free energy landscape, and the error bars represent the 95% confidence intervals calculated from five independent simulations. Note that the free energy landscapes here are only obtained from unbound to bound steady-state WE simulations, and the bound to unbound steady-state WE simulations are required to get the absolute true free energy landscapes.

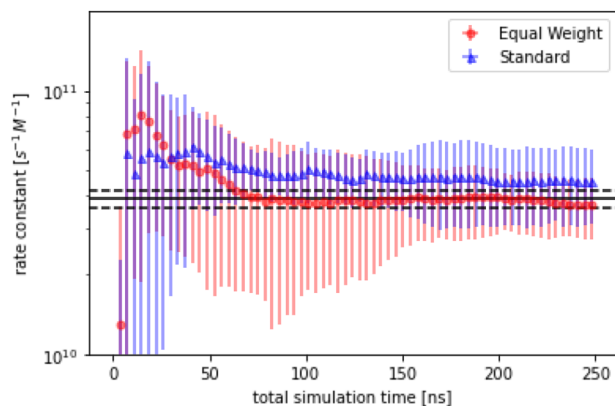


**FIG. 4.** Evolution of the association rate constant from unbound to bound in the  $\text{Na}^+/\text{Cl}^-$  system over 250 ns for both resamplers. The rate constants were calculated based on the RED scheme. The markers represent the average rate constant, and the error bars represent the 95% confidence intervals calculated from five independent simulations. The reference rate constant was  $3.9 \times 10^{10} \pm 0.3 \times 10^{10} \text{ s}^{-1} \text{ M}^{-1}$  based on five  $1 \mu\text{s}$  conventional MD simulations from a previous publication.<sup>41</sup>

unbound to bound steady-state WE simulations, and the bound to unbound steady-state WE simulations are required to get the absolute true free energy landscapes for the  $\text{Na}^+/\text{Cl}^-$  system.

Finally, we compared the resamplers' performance in sampling the association rate constant from unbound to bound in the  $\text{Na}^+/\text{Cl}^-$  system. Figure 4 shows the evolution of the association rate constant over 250 ns for both resamplers. The equal weight resampler converges to the reference rate constant by 75 ns, whereas the standard resampler reaches the reference rate constant within error bounds by 200 ns, which demonstrates the equal weight resampler's efficiency in sampling correct rate constants. Table II shows the final association rate constants and shows that the equal weight resampler is able to obtain a lower relative error than the standard resampler, similar to what was observed for the one-dimensional sinusoidal system. The reverse rate constant cannot be obtained from these particular steady-state WE simulations, which solely focus on sampling the unbound to bound pathways. Overall, with the more complex  $\text{Na}^+/\text{Cl}^-$  system, the equal weight resampler was able to quickly sample the correct free energy landscape and association rate constant and obtain lower simulation errors for both properties compared to the standard resampler.

In summary, our equal weight resampler is able to obtain thermodynamic and kinetic properties more quickly with lower simulation errors from reducing the variance of the trajectories' weights to zero for each bin. The improvement from using the equal weight resampler was especially evident for the more complex  $\text{Na}^+/\text{Cl}^-$  system and for sampling the  $x = 1$  to  $x = 3$  transition in the one-dimensional sinusoidal system that had a high energy barrier. Our comparative study of the equal weight resampler with the standard resampler, which is the first of its kind, along with the study of the effects of increasing the number of bins or target number of trajectories per bin  $n_t$  informed us that having a larger  $n_t$  will proliferate the benefits of using the equal weight resampler, i.e., sampling the correct free energy landscape and rate constants more

**TABLE II.** Final association rate constants for the  $\text{Na}^+/\text{Cl}^-$  system, which represent the average final rate constant from five independent simulations. The error bars represent the 95% confidence intervals calculated from five independent simulations.

Resampler	Rate constant ( $\text{s}^{-1} \text{ M}^{-1}$ )	Relative error (%)
Standard	$4.6 \times 10^{10} \pm 1.4 \times 10^{10}$	30
Equal weight	$3.7 \times 10^{10} \pm 8.8 \times 10^9$	24

quickly and obtaining lower simulation errors. In contrast, a larger number of bins that bridge the different probability regions more effectively lessened the benefits of using the equal weight resampler. Overall, although the improvement from using the equal weight resampler is relatively modest for the two presented systems, the equal weight resampler will be beneficial for any WE simulation in obtaining simulation data more accurately and quickly since the resampler is system agnostic and especially for more complex systems. Our equal weight resampler is available for WESTPA use at [https://github.com/mondrov/Resamplers/blob/main/Equal\\_Weight\\_Resampler](https://github.com/mondrov/Resamplers/blob/main/Equal_Weight_Resampler).

The supplementary material includes additional free energy landscapes and probability flux graphs for the one-dimensional sinusoidal system.

This work was supported by the University of California, Davis. This work used the Expanse supercomputer at the San Diego Supercomputing Center through allocation CHM220013 from the Advanced Cyberinfrastructure Coordination Ecosystem: Services & Support (ACCESS) program, which is supported by the National Science Foundation under Grants Nos. 2138259, 2138286, 2138307, 2137603, and 2138296,<sup>45</sup> and the HPC resources at the Texas Advanced Computing Center (TACC) at the University of Texas at Austin through the Frontera Pathways Allocation. We thank Anthony Bogetti for his helpful discussions and the reviewers for their feedback, which substantially improved the content and the presentation of this paper.

## AUTHOR DECLARATIONS

### Conflict of Interest

The authors have no conflicts to disclose.

### Author Contributions

**Dennis Plotnikov:** Data curation (equal); Formal analysis (equal); Investigation (equal); Software (equal); Validation (equal); Visualization (equal); Writing – original draft (equal). **Surl-Hee Ahn:** Conceptualization (equal); Funding acquisition (equal); Investigation (equal); Methodology (equal); Resources (equal); Supervision (equal); Validation (equal); Writing – review & editing (equal).

### DATA AVAILABILITY

The data that support the findings of this study are available from the corresponding author upon reasonable request.



## REFERENCES

- <sup>1</sup>M. Karplus and J. Kuriyan, *Proc. Natl. Acad. Sci. U. S. A.* **102**, 6679 (2005).
- <sup>2</sup>J. L. Klepeis, K. Lindorff-Larsen, R. O. Dror, and D. E. Shaw, *Curr. Opin. Struct. Biol.* **19**, 120 (2009).
- <sup>3</sup>F. R. Salsbury, Jr, *Curr. Opin. Pharmacol.* **10**, 738 (2010).
- <sup>4</sup>H. Guterres and W. Im, *J. Chem. Inf. Model.* **60**, 2189 (2020).
- <sup>5</sup>D. J. Cole, J. Tirado-Rives, and W. L. Jorgensen, *Biochim. Biophys. Acta* **1850**, 966 (2015).
- <sup>6</sup>S.-H. Ahn, B. R. Jagger, and R. E. Amaro, *J. Chem. Inf. Model.* **60**, 5340 (2020).
- <sup>7</sup>S. M. Ryckbosch, P. A. Wender, and V. S. Pande, *Nat. Commun.* **8**, 6 (2017).
- <sup>8</sup>J. Hu, G.-K. Xu, R. Lipowsky, and T. R. Weikl, *J. Chem. Phys.* **143**, 243137 (2015).
- <sup>9</sup>D. Sabbadin, A. Ciancetta, and S. Moro, *J. Chem. Inf. Model.* **54**, 169 (2014).
- <sup>10</sup>K. Ngo, D. Lopez Mateos, Y. Han, K. C. Rouen, S.-H. Ahn, H. Wulff, C. E. Clancy, V. Yarov-Yarovoy, and I. Vorobyov, *J. Gen. Physiol.* **156**, e202313368 (2024).
- <sup>11</sup>J.-L. Barrat, J. Baschnagel, and A. Lyulin, *Soft Matter* **6**, 3430 (2010).
- <sup>12</sup>M. Yang, V. Koutsos, and M. Zaiser, *J. Phys. Chem. B* **109**, 10009 (2005).
- <sup>13</sup>S.-H. Ahn, J. W. Grate, and E. F. Darve, *J. Chem. Phys.* **149**, 072330 (2018).
- <sup>14</sup>S.-H. Ahn and J. W. Grate, *J. Phys. Chem. B* **123**, 9364 (2019).
- <sup>15</sup>G. M. Torrie and J. P. Valleau, *J. Comput. Phys.* **23**, 187 (1977).
- <sup>16</sup>A. Laio and F. L. Gervasio, *Rep. Prog. Phys.* **71**, 126601 (2008).
- <sup>17</sup>Y. Sugita and Y. Okamoto, *Chem. Phys. Lett.* **314**, 141 (1999).
- <sup>18</sup>Y. Miao, V. A. Feher, and J. A. McCammon, *J. Chem. Theory Comput.* **11**, 3584 (2015).
- <sup>19</sup>E. Darve, D. Rodríguez-Gómez, and A. Pohorille, *J. Chem. Phys.* **128**, 144120 (2008).
- <sup>20</sup>C. Dellago, P. G. Bolhuis, F. S. Csajka, and D. Chandler, *J. Chem. Phys.* **108**, 1964 (1998).
- <sup>21</sup>E. Vanden-Eijnden, M. Venturoli, G. Ciccotti, and R. Elber, *J. Chem. Phys.* **129**, 174102 (2008).
- <sup>22</sup>T. S. Van Erp and P. G. Bolhuis, *J. Comput. Phys.* **205**, 157 (2005).
- <sup>23</sup>G. A. Huber and S. Kim, *Biophys. J.* **70**, 97 (1996).
- <sup>24</sup>V. S. Pande, K. Beauchamp, and G. R. Bowman, *Methods* **52**, 99 (2010).
- <sup>25</sup>D. M. Zuckerman and L. T. Chong, *Annu. Rev. Biophys.* **46**, 43 (2017).
- <sup>26</sup>A. S. Saglam and L. T. Chong, *Chem. Sci.* **10**, 2360 (2019).
- <sup>27</sup>T. Sztain, S.-H. Ahn, A. T. Bogetti, L. Casalino, J. A. Goldsmith, E. Seitz, R. S. McCool, F. L. Kearns, F. Acosta-Reyes, S. Maji *et al.*, *Nat. Chem.* **13**, 963 (2021).
- <sup>28</sup>L. Casalino, A. C. Dommer, Z. Gaieb, E. P. Barros, T. Sztain, S.-H. Ahn, A. Tri-fan, A. Brace, A. T. Bogetti, A. Clyde *et al.*, *Int. J. High Perform. Comput. Appl.* **35**, 432 (2021).
- <sup>29</sup>A. Dommer, L. Casalino, F. Kearns, M. Rosenfeld, N. Wauer, S.-H. Ahn, J. Russo, S. Oliveira, C. Morris, A. Bogetti *et al.*, *Int. J. High Perform. Comput. Appl.* **37**, 28 (2023).
- <sup>30</sup>S. Zhang, J. P. Thompson, J. Xia, A. T. Bogetti, F. York, A. G. Skillman, L. T. Chong, and D. N. LeBard, *J. Chem. Inf. Model.* **62**, 1891 (2022).
- <sup>31</sup>M. C. Zwier, J. L. Adelman, J. W. Kaus, A. J. Pratt, K. F. Wong, N. B. Rego, E. Suárez, S. Lettieri, D. W. Wang, M. Grabe *et al.*, *J. Chem. Theory Comput.* **11**, 800 (2015).
- <sup>32</sup>A. T. Bogetti, B. Mostofian, A. Dickson, A. Pratt, A. S. Saglam, P. O. Harrison, J. L. Adelman, M. Dudek, P. A. Torrillo, A. J. DeGrave *et al.*, *Living J. Comput. Mol. Sci.* **1**, 10607 (2019).
- <sup>33</sup>J. D. Russo, S. Zhang, J. M. Leung, A. T. Bogetti, J. P. Thompson, A. J. DeGrave, P. A. Torrillo, A. Pratt, K. F. Wong, J. Xia *et al.*, *J. Chem. Theory Comput.* **18**, 638 (2022).
- <sup>34</sup>A. T. Bogetti, J. M. Leung, J. D. Russo, S. Zhang, J. P. Thompson, A. S. Saglam, D. Ray, B. Mostofian, A. Pratt, R. C. Abraham *et al.*, *Living J. Comput. Mol. Sci.* **5**, 1655 (2023).
- <sup>35</sup>*Innovations in Biomolecular Modeling and Simulations*, edited by T. Schlick (Royal Society of Chemistry, 2012), Vol. 1.
- <sup>36</sup>D. Aristoff, *J. Appl. Probab.* **59**, 152 (2022).
- <sup>37</sup>D. Aristoff, J. Copperman, G. Simpson, R. Webber, and D. Zuckerman, *J. Chem. Phys.* **158**, 014108 (2023).
- <sup>38</sup>J. A. Izaguirre, D. Thain, and E. Darve, in Proceedings of the SC15 Workshop: Producing High Performance and Sustainable Software for Molecular Simulation, Austin, TX, 2015.
- <sup>39</sup>S.-H. Ahn, J. W. Grate, and E. F. Darve, *J. Chem. Phys.* **147**, 074115 (2017).
- <sup>40</sup>D. A. Case, H. M. Aktulga, K. Belfon, I. Ben-Shalom, S. R. Brozell, D. S. Cerutti, T. E. Cheatham III, V. W. D. Cruzeiro, T. A. Darden, R. E. Duke *et al.*, *Amber 2021* (University of California, San Francisco, 2021).
- <sup>41</sup>P. A. Torrillo, A. T. Bogetti, and L. T. Chong, *J. Phys. Chem. A* **125**, 1642 (2021).
- <sup>42</sup>I. S. Joungh and T. E. Cheatham III, *J. Phys. Chem. B* **112**, 9020 (2008).
- <sup>43</sup>P. Mark and L. Nilsson, *J. Phys. Chem. A* **105**, 9954 (2001).
- <sup>44</sup>A. J. DeGrave, A. T. Bogetti, and L. T. Chong, *J. Chem. Phys.* **154**, 114111 (2021).
- <sup>45</sup>T. J. Boerner, S. Deems, T. R. Furlani, S. L. Knuth, and J. Towns, in *In Practice and Experience in Advanced Research Computing (PEARC '23)* (ACM, Portland, OR, 2023), p. 4.